

# CORRELATION STUDIES ON AN RC FRAME SHAKING-TABLE SPECIMEN

ANGELO D'AMBRISI<sup>1†</sup> AND FILIP C. FILIPPOU<sup>2‡\*</sup>

<sup>1</sup>*Istituto di Scienza delle Costruzioni, Università di Bologna, I-40136 Bologna, Italy*

<sup>2</sup>*Department of Civil Engineering, University of California Berkeley, Berkeley, CA 94720-1710, U.S.A.*

## SUMMARY

This paper presents the correlation of the results of a new model for the dynamic analysis of reinforced concrete (RC) frames with the experimental time history of a two storey RC frame shaking-table specimen. The frame member model consists of separate subelements that describe the deformations due to flexure, shear and bond slip in RC structural elements. The subelements are combined by superposition of flexibility matrices to form the frame element. A non-linear solution method which accounts for the unbalance of internal forces between different subelements during a given load increment is used with the model. The ability of the proposed model to describe the dynamic response of frame structures under earthquake excitations is evaluated by comparing the analytical results with experimental evidence from a two-storey, one bay reinforced concrete frame tested on the shaking-table. The model parameters for the shaking-table specimen are derived from available experimental evidence and first principles of reinforced concrete. The effect of reinforcing bar slip on the local and global dynamic response of the test structure is assessed. © 1997 John Wiley & Sons, Ltd.

*Earthquake Engng. Struct. Dyn.*, **26**, 1021–1040 (1997)

No. of Figures: 10. No. of Tables: 4. No. of References: 17.

KEY WORDS: non-linear dynamic analysis; RC frames; shaking table; non-linear beam element; reinforcing bar slip

## INTRODUCTION

In Reinforced Concrete (RC) frame structures, designed according to current specifications of earthquake-resistant design, forces and displacements are expected to exceed greatly those induced by the equivalent static lateral loads stipulated in codes. When these structures are subjected to severe earthquake excitations they are expected to deform well into the inelastic range and dissipate the large seismic energy input into the structure through large but controllable inelastic deformations at critical regions. In order to predict the distribution of forces and deformations in these structures under the maximum credible earthquake that can occur at the site, accurate models of the hysteretic behaviour of the different critical regions of the structure are necessary.

Many analytical models have been proposed to date for the non-linear analysis of reinforced concrete frame structures. These range from very refined and complex local models to simplified global models.

\* Correspondence to: F. C. Filippou, Department of Civil Engineering, University of California, MC 1710, Berkeley, CA 94720-1710 U.S.A.

† Research Assistant

‡ Associate Professor

Contract grant sponsor: National Science Foundation; Contract grant number: ECE-8657525  
Contract grant sponsor: CNR; Contract grant number: 94. 01898. CT07

Refined analytical models are typically used in predicting the response of small structures or structural subassemblies.<sup>1</sup> On the other hand, simplified global models have been typically used in the dynamic response analysis of large structures.<sup>2–4</sup>

The major sources of deformation in reinforced concrete frame structures are flexural rotation, shear deformation, including shear sliding, and bond slip. The hysteretic load–deformation behaviour of frame members arises from a combination of these deformation mechanisms. A rational analysis of the hysteretic behaviour of reinforced concrete members needs to be based on the description of all deformation sources and of the interactions between the different mechanisms.<sup>5</sup> This approach permits the determination of the relative contribution of each source of inelastic behaviour to the local and global response of reinforced concrete frames. In order to achieve this goal, new frame member models have been recently proposed.<sup>6</sup> In these models, each frame member is made up of different subelements. Each subelement represents a different source of inelastic behaviour. The parameters of the subelements are established from first principles, or, otherwise from experimental information or local finite element models. The proposed frame idealization<sup>6</sup> is complex enough to approximate the behaviour of the real structure, yet simple enough to be practical in the non-linear dynamic analysis of large structures.

In this paper the performance of the new frame models is discussed in the context of the non-linear dynamic analysis of a two-storey shaking-table test frame. After a brief introduction of the salient features of the frame models and the non-linear algorithm that ensures compatibility and equilibrium between the component elements of a frame member, their performance is evaluated by comparing the analytical results with experimental evidence from a shaking-table study of a two storey, one bay reinforced concrete frame.<sup>7</sup> In this structure reinforcing bar slip at the base of the columns played an important role in the global response. This effect is, therefore, evaluated in some detail in this paper.

### MODELING ASSUMPTIONS

For the accurate description of the non-linear dynamic response of RC frame structures three-dimensional models are the best solution. At present the refined three-dimensional dynamic analysis of RC buildings is computationally intensive. This study is limited to two-dimensional models of symmetric buildings along one principal axis and determines the response of these models to a ground motion whose direction coincides with this axis. The features of the proposed two-dimensional model are summarized below (Figure 1):

- (a) One vertical degree of freedom and one rotational degree of freedom per node as well as one horizontal degree of freedom per floor is assumed.
- (b) The building mass is assumed to be lumped at the floors. Mass is assigned to the lateral translational degrees of freedom only, and the rotational inertia is not accounted for.
- (c) Only horizontal ground accelerations are considered.
- (d) Gravity loads are included in the analysis as fixed moments and shear forces at the girder ends. Joint loads are directly applied as concentrated moments and forces at the nodes. A static analysis is performed before the beginning of the dynamic response analysis.
- (e) The model includes inelastic deformations in girders and columns with due account of the effect of axial load on stiffness and strength.
- (f) Shear effects in girders and columns, the axial deformations of columns and second-order deformations due to  $P - \Delta$  effects are included in the analysis.
- (g) Finite joint dimensions are used in determining the clear span of members. Fixed end rotations at the beam–column and column–foundation interface due to bond deterioration in the anchorage zone are taken into account.
- (h) The addition of rotational springs at the base of the columns can simulate the condition of hinged, partially fixed or completely fixed supports. Translational springs at the base of the building can simulate sliding, rocking, and settlement of the foundation.

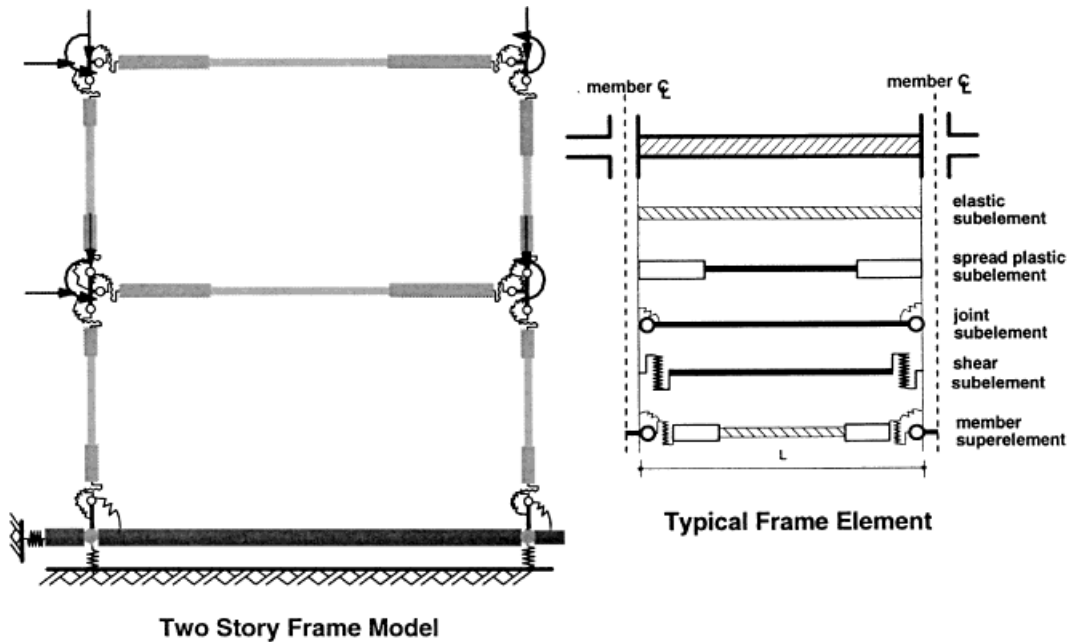


Figure 1. Plane frame modeling and typical frame element with components

- (i) The frame members are assumed to have infinite ductility, so that failure by attainment of the actual ultimate strength or deformation capacity of the member is not considered.

The formulation of the frame element model is briefly discussed in the following.

### NON-LINEAR DYNAMIC ANALYSIS

The incremental equations of dynamic equilibrium for a multi-degree of freedom system are<sup>8</sup>

$$\mathbf{M}\Delta\ddot{\mathbf{r}} + \mathbf{C}\Delta\dot{\mathbf{r}} + \mathbf{K}_T\Delta\mathbf{r} = \Delta\mathbf{R} \quad (1)$$

where  $\Delta\mathbf{r}$ ,  $\Delta\dot{\mathbf{r}}$  and  $\Delta\ddot{\mathbf{r}}$  are the increments of displacement, velocity and acceleration vectors during the time step  $\Delta t$ , respectively.  $\mathbf{M}$ ,  $\mathbf{C}$  and  $\mathbf{K}_T$  are the mass, damping, and tangent stiffness matrix, respectively, and  $\Delta\mathbf{R}$  is the increment of external loads during the time step  $\Delta t$ . For base acceleration,  $\Delta\mathbf{R}$  is given by  $\Delta\mathbf{R} = -\mathbf{M}\cdot\mathbf{1}\cdot\Delta\ddot{a}_g$ , where  $\mathbf{1}$  is a unit vector and  $\Delta\ddot{a}_g$  is the base acceleration increment during time step  $\Delta t$ .

A lumped mass matrix  $\mathbf{M}$  is assumed in the analysis. Non-zero diagonal terms are associated only with translational degrees of freedom and remain constant during the dynamic response. The damping matrix  $\mathbf{C}$  is assumed to be proportional to the initial stiffness  $\mathbf{K}_0$  and mass matrix  $\mathbf{M}$  according to

$$\mathbf{C} = \alpha\mathbf{M} + \beta\mathbf{K}_0 \quad (2)$$

Constants  $\alpha$  and  $\beta$  are determined by selecting suitable damping ratios for two vibration modes.<sup>8</sup>

The tangent stiffness matrix  $\mathbf{K}_T$  is derived by direct assembly of the stiffness matrices of the individual frame elements. The determination of the element stiffness matrix is described in the following section.

The incremental equations of dynamic equilibrium in equation (1) are integrated with the Newmark Constant Acceleration Method<sup>8</sup> which transforms equation (1) to the following incremental relation:

$$\mathbf{K}_e \Delta \mathbf{r} = \Delta \mathbf{R}_e \tag{3}$$

where  $\mathbf{K}_e$  is the effective stiffness matrix and  $\Delta \mathbf{R}_e$  is the effective load increment. Expressions for  $\mathbf{K}_e$  and  $\Delta \mathbf{R}_e$  can be found in most textbooks on structural dynamics (e.g. see Reference 8).

### RC FRAME ELEMENT MODEL

In the proposed model the frame member is decomposed into different subelements. Each subelement describes a different deformation mechanism that affects the hysteretic behaviour of critical regions in girders and columns. In the column subelements, the interaction of axial load, bending moment and shear force with the opening and closing of the cracks is taken into account. Furthermore, the column element also includes axial deformations and geometric  $P - \Delta$  effects. The following member subelements are used in the correlation studies in this paper (Figure 1): (1) an elastic subelement; (2) a spread plastic subelement; (3) a joint (fixed-end rotation) subelement. The shear subelement is not included in the discussion, because shear deformations were not significant in the two-storey test frame.

The linear elastic subelement represents the flexural behaviour of the frame member before yielding of the reinforcement. The spread rigid-plastic subelement represents the inelastic flexural deformation of the member after yielding of the reinforcement. It consists of one inelastic zone at each end and an infinitely rigid bar connecting these, as shown in Figure 2(a). The gradual spread of inelastic flexural deformations into the member as a function of loading history is described by the gradually increasing length of the inelastic zone. The hysteretic behaviour of the element depends on the moment–curvature relation of the inelastic zones in Figure 2(b). It does not include any ‘pinching’, which can be attributed to sliding and bond-slip deformations in RC members. These deformations are included in the fixed-end rotation and shear subelement. The primary curve of the moment–curvature relation includes the effect of axial load, but does not account for its variation. The flexibility matrix of the spread plastic subelement contains off-diagonal terms due to the shift of the point of zero moment that results in coupling of end moments. This distinguishes the element from the one-component model.<sup>9</sup>

The joint subelement represents the fixed-end rotation at the beam to column interface or the column to footing interface due to reinforcing bar slip in the anchorage zone. The joint element does not account for deformation due to reinforcement slip along the frame member. This deformation is, however, included in the

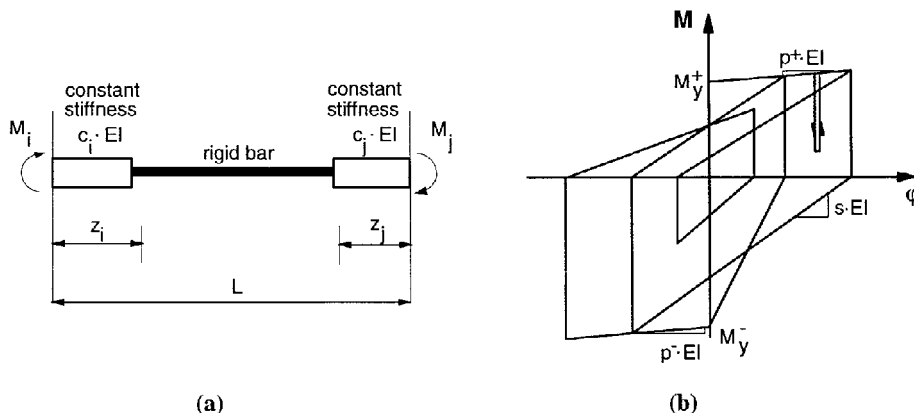


Figure 2. Spread rigid plastic subelement

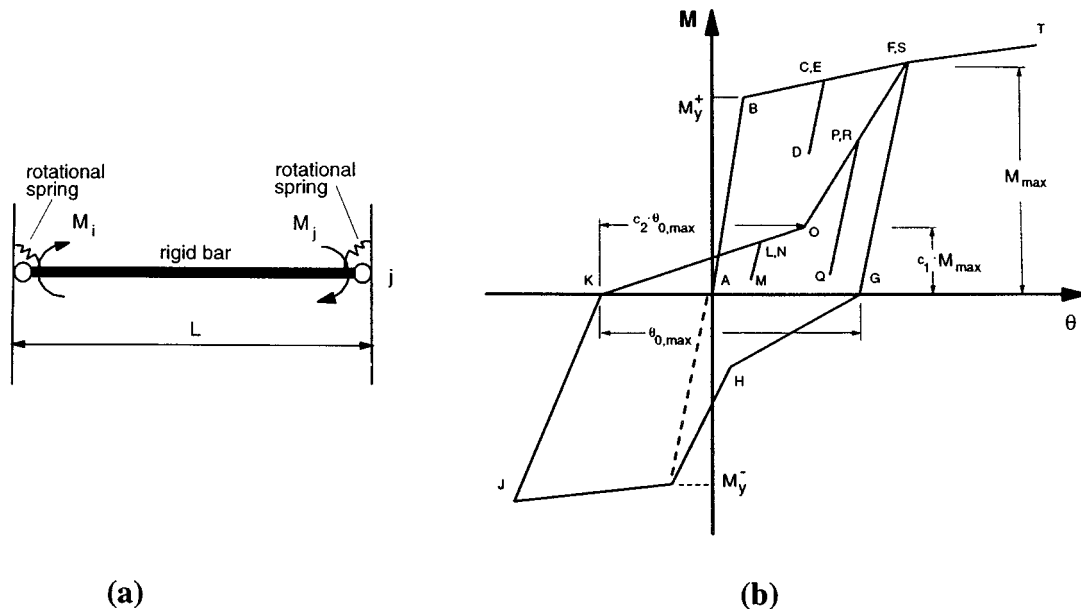


Figure 3. Joint (fixed-end rotation) subelement

spread plastic subelement in the form of an average curvature distribution in each inelastic zone. The joint subelement is represented by two rotational springs connected with a rigid bar in Figure 3(a). The hysteretic behaviour of the springs governs the hysteretic response of the element. The primary curve of the moment-fixed-end rotation relation in Figure 3(b) accounts for the effect of axial load, as described in more detail in Reference 6. It is governed by the following rules: (1) A bilinear elastic-strain hardening envelope curve (ABC) describes the monotonic behaviour. (2) A constant stiffness is assumed until the end section reaches the yield moment  $M_y$ . (3) Unloading takes place along a line FG parallel to the initial stiffness. (4) Upon reloading in a direction with previous inelastic deformation, there is a significant reduction in stiffness caused by the open crack. This stiffness remains in effect until the crack closes (point O). The point at which the crack closes, is determined by parameters  $c_1$  and  $c_2$  in Figure 3(b). These parameters control the 'pinching' of the hysteretic moment-rotation relation and depend on the axial force. The amount of 'pinching' increases with increasing axial load. Values for these factors are derived with a special purpose joint model.<sup>6</sup> (5) Once the crack closes at point O, reloading follows a straight line connecting point O with the point of maximum previous rotation on the envelope curve (point S in Figure 3(b)). (6) In the case of partial unloading followed by reloading, the loading stiffness is parallel to the elastic stiffness until the point at which unloading started is reached (C-D-E), (L-M-N), (P-Q-R).

Equilibrium considerations require that the constituent subelements of the frame member experience the same end moments. The subelements are, therefore, connected in series, so that the tangent flexibility matrix of the frame member  $F_m$  is simply the sum of the tangent flexibility matrices of the subelements. The tangent member stiffness  $K_m$  in local co-ordinates is the inverse of the tangent flexibility matrix. It is transformed to global co-ordinates after the addition of rigid-body modes and directly assembled into the tangent stiffness matrix of the structure by well established procedures of structural analysis. Further details are given in Reference 6.

### NUMERICAL IMPLEMENTATION

At the beginning of each step of the time integration algorithm the current effective stiffness  $\mathbf{K}_e$  and load vector increment  $\Delta \mathbf{R}_e$  in equation (3) is established. The solution of equation (3) yields the current displacement increments  $\Delta \mathbf{r}$ . From  $\Delta \mathbf{r}$  the deformation increments  $\Delta \mathbf{r}_m$  at the ends of each element of the structure can be extracted. The transformation of the deformation increments  $\Delta \mathbf{r}_m$  to the local reference system without rigid-body modes yields the rotation increments  $\Delta \Theta$  at the element ends.

The corresponding moment increments at the element ends are determined with the current element stiffness matrix  $\mathbf{K}_m$  according to

$$\Delta \mathbf{M}_m = \mathbf{K}_m \Delta \Theta \quad (4)$$

Since the frame member subelements are connected in series, the end moments  $\Delta \mathbf{M}_m$  yield directly the end moment increments  $\Delta \mathbf{m}$  for each subelement:

$$\Delta \mathbf{M}_m = \Delta \mathbf{m}_{el} = \Delta \mathbf{m}_{pl} = \Delta \mathbf{m}_{jnt} \quad (5)$$

The end moment increments  $\Delta \mathbf{m}$  and the current flexibility matrix  $\mathbf{f}$  of each subelement yield the current end rotation increments of the subelement

$$\Delta \theta = \mathbf{f} \Delta \mathbf{m} \quad (6)$$

At this point each subelement performs a state determination which updates the end rotations and determines the increment of end resisting moments  $\Delta \mathbf{m}_R$ . If the difference between externally applied moment increments  $\Delta \mathbf{m}$  and resisting moment increments  $\Delta \mathbf{m}_R$  is larger than a specified tolerance for any subelement, the flexibility matrix of the corresponding subelement is updated to  $\mathbf{f}_u$ . The inverse of the new flexibility matrix yields the updated stiffness matrix  $\mathbf{k}_u$  and initial end moment increments  $\Delta \mathbf{m}_0$  for each subelement according to

$$\Delta \mathbf{m}_0 = \Delta \mathbf{m}_R - \mathbf{k}_u \Delta \theta \quad (7)$$

Once the initial moment increments of all subelements are determined, the initial moment increments of the entire frame element are established from the following relation:

$$\Delta \mathbf{M}_0 = \mathbf{K}_{mu} \{ \mathbf{f}_{u,pl} \Delta \mathbf{m}_{0,pl} + \mathbf{f}_{u,jnt} \Delta \mathbf{m}_{0,jnt} \} \quad (8)$$

where pl stands for spread rigid plastic subelement, jnt stands for joint subelement and  $\mathbf{K}_{mu}$  is the updated member stiffness. The initial moments of each frame element are transformed to global co-ordinates, assembled in the global force vector and subtracted from the effective load increments  $\Delta \mathbf{R}_e$  of the current time step. The resulting unbalanced force vector replaces  $\Delta \mathbf{R}_e$  in equation (3) and new displacement increments are determined with the updated structure stiffness matrix. This iteration process continues within a time step until the norm of the unbalance force vector is smaller than a specified tolerance. The frame element state determination in equations (4)–(8) ensures that moment equilibrium and rotation compatibility is always satisfied at the element ends.<sup>6</sup> The global iteration process ensures that structure equilibrium and inter-element compatibility is satisfied upon convergence of the iteration process within a time step. This algorithm proved to be accurate and computationally efficient in non-linear seismic response studies of multistorey frames.<sup>10</sup>

### NONLINEAR DYNAMIC RESPONSE OF TEST FRAME

The ability of the model to describe the dynamic response of RC frame structures under earthquake ground motion is assessed by correlation of analytical results with experimental evidence from a two-storey, one bay RC frame that was subjected to a simulated strong base motion. The test specimen referred to as RCF2 is a 0.7 scale model of a two-storey office building representative of common design and construction practice.<sup>7</sup>

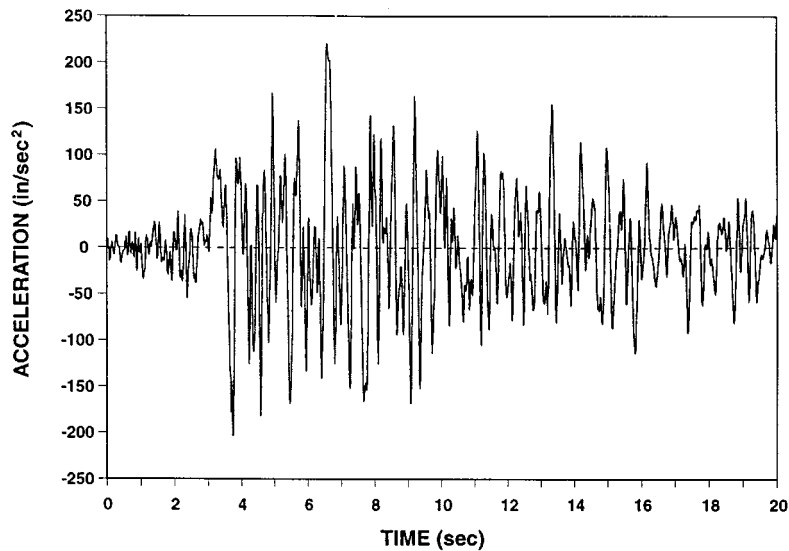


Figure 4. N69W taft accelerogram record, 21 July 1952, scaled to 0.57g

The frame was designed according to 1970 UBC and 1971 ACI Code of practice and the design was later verified with 1979 UBC Code.<sup>11</sup> Another analytical study has also used the frame response as reference.<sup>12</sup>

The test frame was subjected to three consecutive base acceleration histories on the shaking table of UC Berkeley. All motions correspond to the N69W Taft record from the Arvin-Tahachapi earthquake of 21 July 1952, scaled to peak accelerations of 0.095g, 0.57g (Figure 4), and 0.65g. The three tests were referred to as W1, W2, and W3, respectively. This study refers only to test W2, because it refers to the response of an essentially undamaged building to a base acceleration that is severe enough to cause significant concrete damage and yielding of the reinforcing steel. At the start of the test, the test frame was slightly cracked from the previous test W1, as actual structures in service might be.

#### DETERMINATION OF MEMBER PROPERTIES OF TEST FRAME RCF2

The geometry and reinforcing details of the test frame and as well as the arrangement on the shaking table and the conduct of the test are described in Reference 7. A very difficult task in the correlation between experimental and analytical results is the selection of the model properties representing the state of the specimen at the beginning of the test. Moreover, from a practical viewpoint, the results of the correlation are only meaningful if the model properties can be derived by first principles from information that is readily available during the design of a reinforced concrete structure without ad hoc assumptions.

Because of the inherent uncertainty about the physical state of the test specimen and the actual physical and mechanical characteristics of the materials in the as-built specimen, the attempt was made first to establish a reasonable range for each parameter value. This was accomplished with the information about the geometry of the test specimen and the actual material characteristics given by Clough and Gidwani.<sup>7</sup> Within this range a trial and error process to obtain satisfactory response agreement led to the set of parameter values that was used throughout the correlation studies and is reported in Tables I–IV.

At the start of the second shaking-table run W2 test frame RCF2 was reportedly undamaged although slightly cracked. Thus, the selection of initial stiffness for the members of the frame model depends on the state of cracking of the test frame members. The initial stiffness of the frame model establishes its fundamental

Table I. Member properties of bottom storey girders in analytical model

RCF2 frame—bottom-storey girders							
		Spread plasticity model		Concentrated plasticity model		Joint	
		Girder moment–curvature relation		Girder moment–rotation relation		Moment–rotation relation	
Yield moments (k in)		Initial stiffness (10 <sup>3</sup> k in <sup>2</sup> /rad)	Strain-hardening ratio	Initial stiffness (10 <sup>3</sup> k in/rad)	Strain-hardening ratio	Initial stiffness (10 <sup>3</sup> k in/rad)	Strain-hardening ratio
M <sup>+</sup>	232	1531	0.012	1531	0.025	200	0.04
M <sup>-</sup>	720	1531	0.020	1531	0.038	200	0.04

Table II. Member properties of top-storey girders in analytical model

RCF2 frame—top-storey girders							
		Spread plasticity model		Concentrated plasticity model		Joint	
		Girder moment–curvature relation		Girder moment–rotation relation		Moment–rotation relation	
Yield moments (k in)		Initial stiffness (10 <sup>3</sup> k in <sup>2</sup> /rad)	Strain-hardening ratio	Initial stiffness (10 <sup>3</sup> k in/rad)	Strain-hardening ratio	Initial stiffness (10 <sup>3</sup> k in/rad)	Strain-hardening ratio
M <sup>+</sup>	205	1188	0.012	1188	0.025	200	0.04
M <sup>-</sup>	640	1188	0.020	1188	0.038	200	0.04

Table III. Member properties of bottom-storey columns in analytical model

RCF2 frame—bottom-storey columns							
		Spread plasticity model		Concentrated plasticity model		Joint	
		Girder moment–curvature relation		Girder moment–rotation relation		Moment–rotation relation	
Yield moments (k in)		Initial stiffness (10 <sup>3</sup> k in <sup>2</sup> /rad)	Strain-hardening ratio	Initial stiffness (10 <sup>3</sup> k in/rad)	Strain-hardening ratio	Initial stiffness (10 <sup>3</sup> k in/rad)	Strain-hardening ratio
M <sup>+</sup>	208	390	0.03	390	0.05	50	0.04
M <sup>-</sup>	208	390	0.03	390	0.05	50	0.04

period of vibration at test initiation. For test frame RCF2 the fundamental period at test initiation is close to the range of period values with significant energy input of the base motion in Figure 5. This 'tuning' between test structure and base excitation makes the initial stiffness selection of the members in the model a determining factor of the quality of the non-linear response correlation.

Table IV. Member properties of top storey columns in analytical model

RCF2 frame—bottom-storey girders							
		Spread plasticity model		Concentrated plasticity model		Joint	
		Girder moment–curvature relation		Girder moment–rotation relation		Moment–rotation relation	
Yield moments (k in)		Initial stiffness ( $10^3$ k in <sup>2</sup> /rad)	Strain-hardening ratio	Initial stiffness ( $10^3$ k in/rad)	Strain-hardening ratio	Initial stiffness ( $10^3$ k in/rad)	Strain-hardening ratio
M <sup>+</sup>	194	500	0.03	500	0.05	60	0.04
M <sup>-</sup>	194	500	0.03	500	0.05	60	0.04

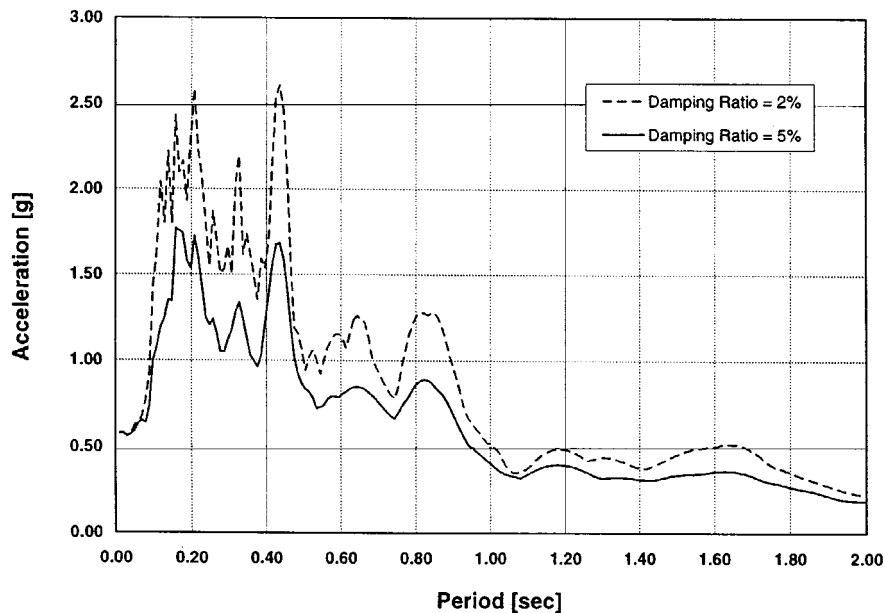


Figure 5. Acceleration response spectrum for shaking table test W2

The stiffness selection was aided by the thorough measurements of the overall stiffness of the test frame prior to the start of run W2.<sup>7</sup> These tests consisted of the measurement of individual flexibility coefficients of the two-storey test frame and of snap tests. The measured flexibility coefficients yield values of  $f_1 = 1.92$  Hz and  $f_2 = 6.06$  Hz for the first and second vibration mode, respectively. These values are lower than the corresponding values from the snap tests which were  $f_1 = 2.03$  Hz and  $f_2 = 6.70$  Hz for the first and second vibration mode, respectively. The discrepancy between these two sets of values is about 6 per cent, but no explanation for this deviation is recorded.<sup>7</sup> At the end of test run W2 the corresponding frequency values from the snap test were  $f_1 = 1.88$  Hz and  $f_2 = 6.14$  Hz for the first and second vibration mode, respectively. This frequency shift can be attributed to damage at the first-storey column ends, while the girders and second-storey columns did not suffer damage.

Since the snap test values appear more reliable, it was decided to use the values of  $f_1 = 2.03$  Hz and  $f_2 = 6.70$  Hz as the reference values to match. With an initial member stiffness equivalent to fully cracked conditions and with concrete modulus  $E_c$  equal to the measured mean value from cylinder tests, the frequency values of the frame model were  $f_1 = 2.19$  Hz and  $f_2 = 5.73$  Hz. The good agreement between analytical and snap test frequencies suggests that the selected stiffness values represent reasonably well the state of the two-storey frame before run W2.

The damping ratios from the snap tests before run W2 were  $\xi_1 = 5.77$  per cent and  $\xi_2 = 2.99$  per cent for the first and second vibration mode, respectively. At the completion of test W2 these values increased to  $\xi_1 = 6.56$  per cent and  $\xi_2 = 3.46$  per cent. In the analytical studies a damping ratio of 5 per cent of critical was assumed for the first two vibration modes to account for viscous damping.

The yield moment values for bottom- and top-storey girders in Tables I and II, respectively, account for the effective floor slab width and the effect of compression reinforcement. For the determination of column yield strength two significantly different axial force-bending moment interaction diagrams are presented by Clough and Gidwani<sup>7</sup> and in a later study by Blondet *et al.*<sup>11</sup> The latter interaction diagram was adopted in this study, since it is more consistent with experimental evidence about the test frame behaviour. The column yield strength values in Tables III and IV are based on an increase of 25 per cent of the nominal yield strength of reinforcing steel ( $f_y = 1.25 \cdot 40$  ksi = 50 ksi) and without the strength capacity reduction factor of  $\phi = 0.70$ . The resulting yield strength represents the upper bound in the study by Blondet *et al.*<sup>11</sup> and results in a maximum base shear that is about 18 per cent lower than the measured value. The column yield strength values in Tables III and IV correspond to an axial force from the action of gravity loads in the test frame. The hysteretic behaviour of the column subelements does not account for the variation of axial force due to overturning effects. This is a reasonable approximation for the two-storey test frame with small height to base width ratio, but may result in large errors in the dynamic response of high-rise building frames. In the latter case, it is recommended to use fibre beam-column elements to simulate the hysteretic behaviour of RC columns.<sup>13</sup> The strain hardening values of the moment-curvature relation for girders and columns are straightforward to calculate from first principles of RC design.

The parameters of the joint subelements in Tables I–IV are derived with the simple assumption of an average effective bond stress along the anchorage, as recommended by Park and Paulay.<sup>14</sup> The strain hardening values of the joint moment-rotation relation are obtained with a simple anchorage model.<sup>15</sup> Calculation details are given in Reference 16. It is characteristic that the strain-hardening values in Tables I–IV vary over the small range of 0.012–0.05 in good agreement with values used in previous related studies.<sup>7,17</sup> These values are primarily affected by the strain-hardening ratio of reinforcing steel, with bond representing the second most important effect.

## CORRELATION WITH EXPERIMENTAL RESULTS

During shaking-table run W2, the specimen was subjected to simulated gravity loading, and a shaking-table signal that corresponded to the N69W Taft accelerogram record during the Arvin-Tahachapi earthquake of 21 July 1952 (Figures 4 and 5). The Taft signal was amplified to a table motion with a peak acceleration of  $0.57g$  that was strong enough to produce significant damage to the specimen. Moreover, the fundamental period of the frame at the beginning of the test was approximately equal to 0.5 sec and, thus, was close to the period range of significant energy input of the ground motion, as the acceleration response spectrum shows in Figure 5. The small size of the test frame prevented the development of any significant shaking-table-test frame interaction, so that this effect is not included in the following analytical results.

The model of the test frame consists of two girder and four column elements, each with a linear elastic, spread rigid-plastic and joint subelement. Since the response of this particular structure is dominated by flexure and reinforcing bar slip and shear deformations are not significant, the shear subelement was not included in the following analyses. The following time histories are compared with experimental data: the bottom and top floor displacement in Figures 6(a) and 6(b); the top interstorey drift in Figure 6(c), and the top

and bottom storey shear in Figures 6(d) and 6(e). A careful study of these comparisons in Figure 6 yields the following observations:

- (1) In general, very satisfactory agreement between experimental and analytical results is observed. The period and general waveform of the response is represented well with the proposed model. This is an indication that the model matches well the actual strength and stiffness of the structure. In particular, the following model features are instrumental to the good agreement between analytical and experimental results: (a) the strain-hardening stiffness of the members is not constant but decreases with increasing deformation; (b) the hysteretic moment–rotation relation at each member end changes with loading history, because of coupling between the response at the two member ends. Thus, the moment–rotation relation at one end of the member depends on section stiffness and plastic zone length at the other end; (c) the post yield stiffness of the model is not based on the assumption that the point of inflection is fixed at the member midspan as the one-component model postulates. The post yield stiffness of each member varies with the actual moment distribution during the response time history; (d) the bond deterioration and slip of reinforcing steel is taken into account as a major source of energy dissipation; (e) the hysteretic behaviour of the members accounts for the stiffness degradation due to crack opening and closing and slip of reinforcing steel.
- (2) The displacement time histories in Figures 6(a)–6(c) show very good agreement, but the correlation is better for the top and bottom displacement than for the top-storey drift which is the difference of two displacement values.
- (3) The storey shear response history agrees quite well with experimental results in Figures 6(d) and 6(e), but this agreement is not as good as for the displacements. However, some questions about the reliability of the measured storey shear values were raised.<sup>7</sup>
- (4) The higher mode effects are much more prominent in the top-storey shear than in the bottom-storey shear response in Figures 6(d) and 6(e).
- (5) The maximum response values for the top- and bottom-storey displacement, top interstorey drift, and top- and bottom-storey shear agree very well between experiment and analysis.

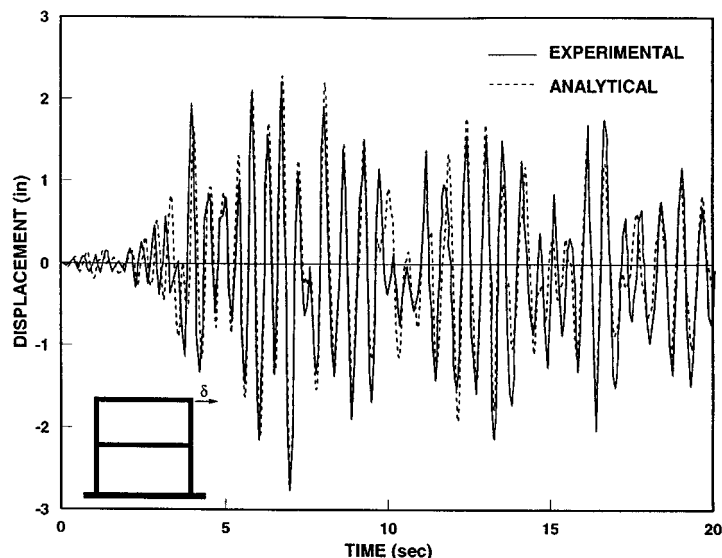


Figure 6(a). Correlation of top-storey displacement response

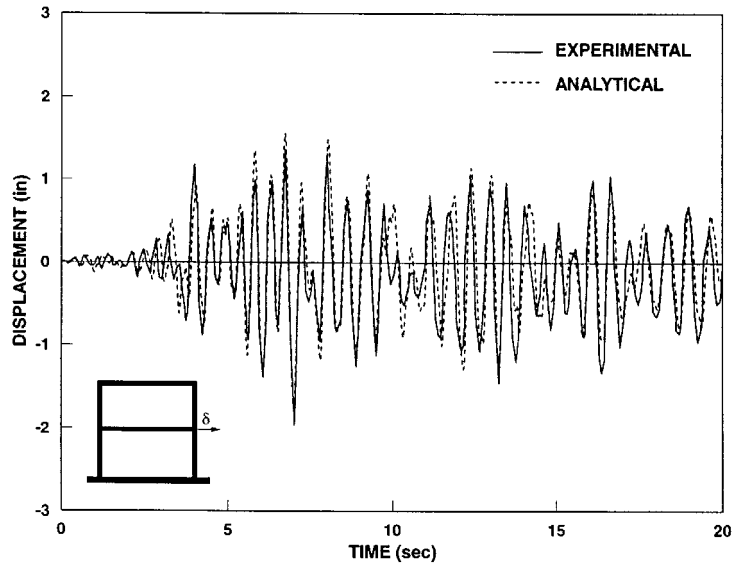


Figure 6(b). Correlation of bottom-storey displacement response

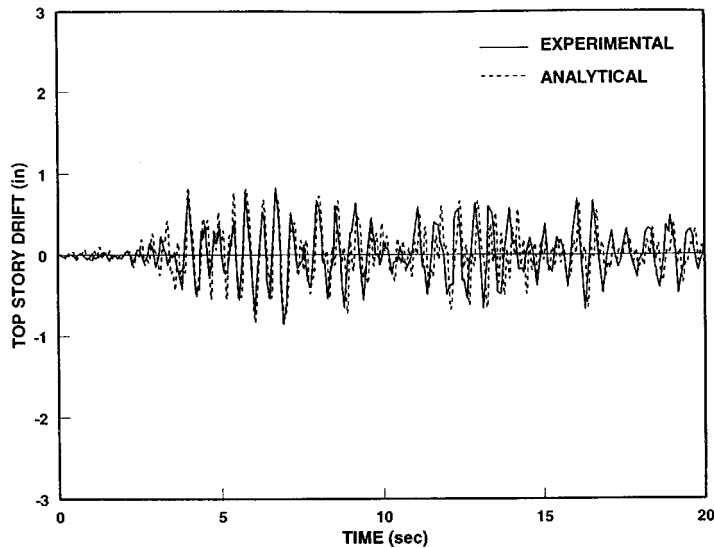


Figure 6(c). Correlation of top-storey drift response

- (6) In spite of the quite satisfactory correlation between experiment and analysis, a slight phase shift appears at the last stages of the response time history and results in a noticeable discrepancy between experimental and analytical results in the last few cycles in Figure 6. This discrepancy can be attributed to the following facts: (a) the limitations of the relatively simple model in describing the damage evolution in the actual structure, (b) the complexity of the behaviour of the damaged RC test frame and

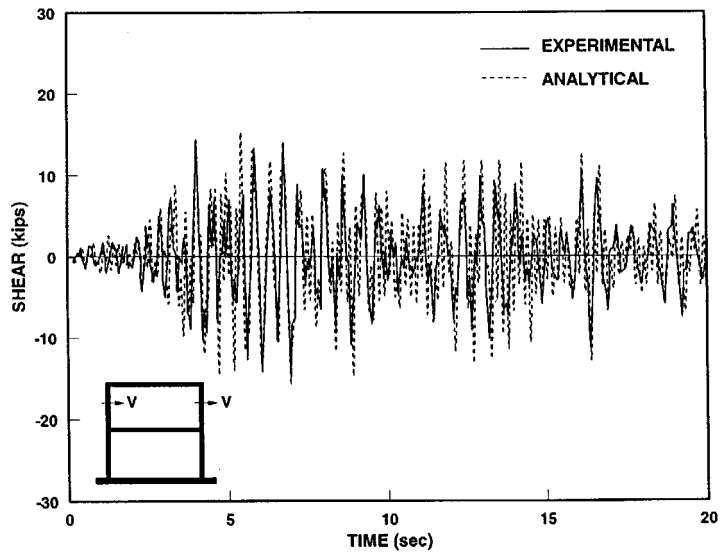


Figure 6(d). Correlation of top-storey shear response

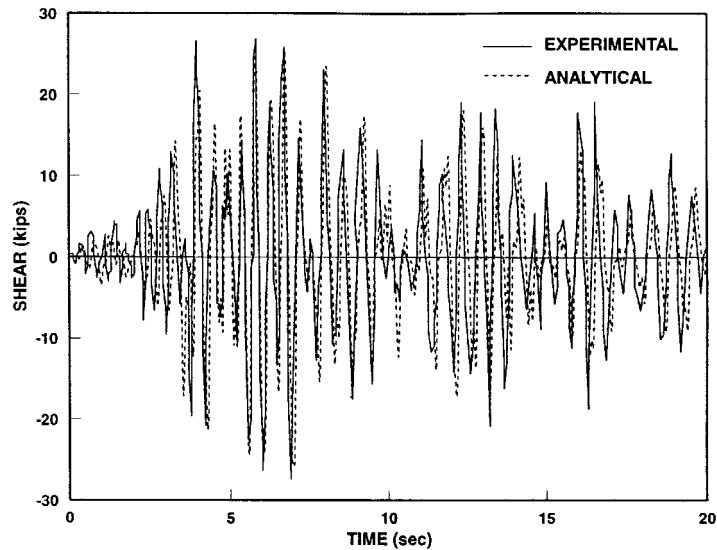


Figure 6(e). Correlation of bottom-storey shear response

(c) the uncertainty in the determination of actual material properties and in the data acquisition during the test.

#### EFFECT OF REINFORCING BAR SLIP ON THE DYNAMIC RESPONSE OF TEST FRAME

In this section the dynamic responses of the test frame with and without the effect of reinforcing bar slip are compared in order to study the sensitivity of the results to this parameter. In test frame RCF2 the reinforcing

bar slip is most pronounced as fixed-end rotation at the base of the first-storey columns. The reinforcing bar slip was much smaller at the top of the columns and was practically insignificant at the girder ends, since the latter did not yield. In the following studies the joint subelement is turned on or off for including or excluding the effect of reinforcing bar slip, respectively. Figure 7 shows the displacement and storey shear time history of the shaking table specimen to the N69W Taft accelerogram scaled to a peak acceleration of  $0.57g$ . The maximum top-storey displacement in Figure 7(a) is about 50 per cent larger when the effect of reinforcing bar slip

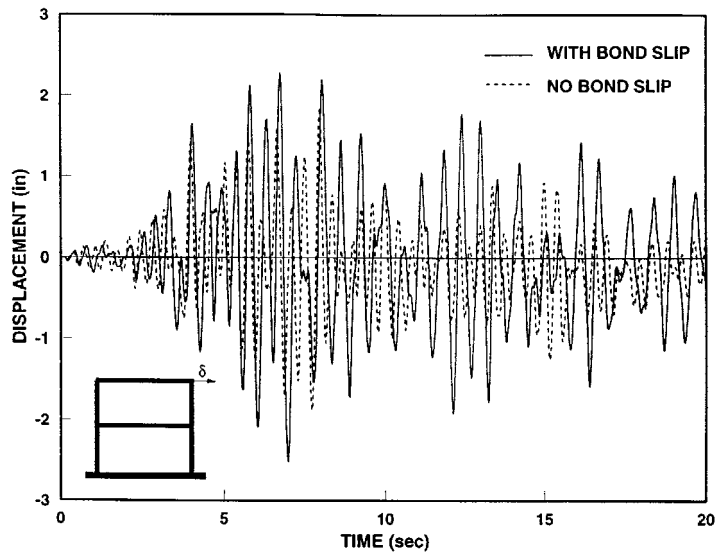


Figure 7(a). Effect of bar slip on top-storey displacement

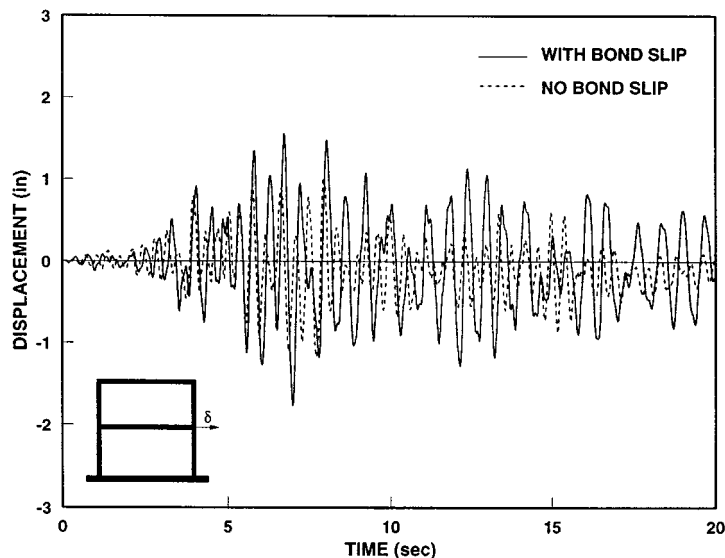


Figure 7(b). Effect of bar slip on bottom-storey displacement

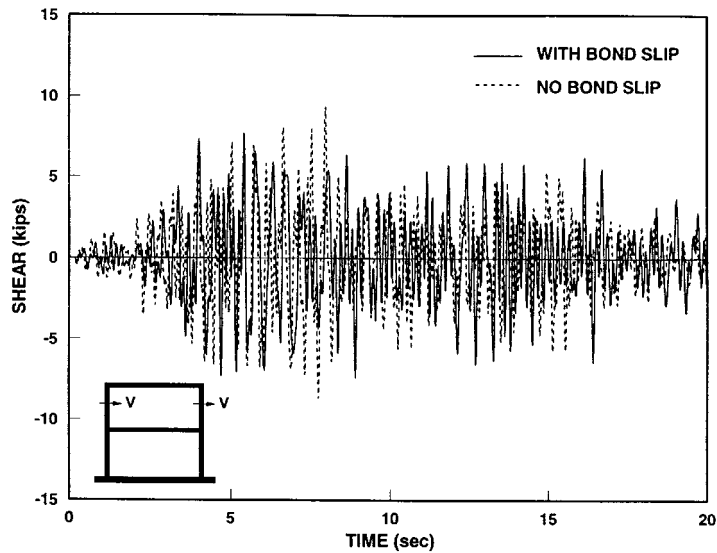


Figure 7(c). Effect of bar slip on top-storey shear

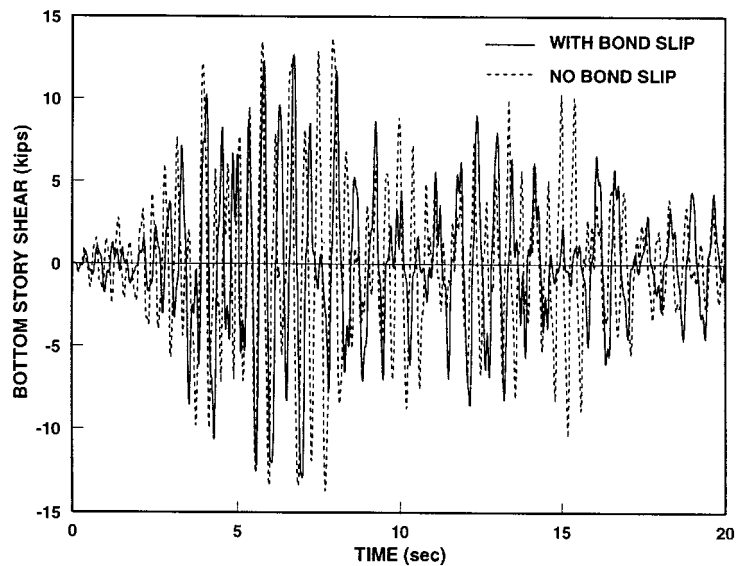


Figure 7(d). Effect of bar slip on bottom-storey shear

slip is included. The difference in the displacement time history is equally pronounced for the bottom-storey displacement in Figure 7(b). The response of the model without reinforcing bar slip clearly exhibits a shorter period of vibration. A comparison of Figure 7(a) with Figure 7(b) reveals that the difference of maximum displacements between the two cases is approximately the same for the top- and bottom-storey displacement. This confirms that most of the inelastic deformation of the two-storey test frame arises in the bottom storey

and that the effect of joint rotations is almost exclusively concentrated at the base of the frame in the form of pull-out deformations from the footing.

The displacement time histories in Figures 7(a) and 7(b) reveal that the response of the model without the effect of bond slip dies out in the last 5 sec of the test. By contrast, the model that includes this effect continues to respond strongly to the base signal, in good agreement with the experimental evidence in Figures 6(a) and 6(b). It is of interest to note that previous studies dealing with the dynamic response of test frame RCF2 have failed to capture this effect, because of their inability to represent correctly the different mechanisms of energy

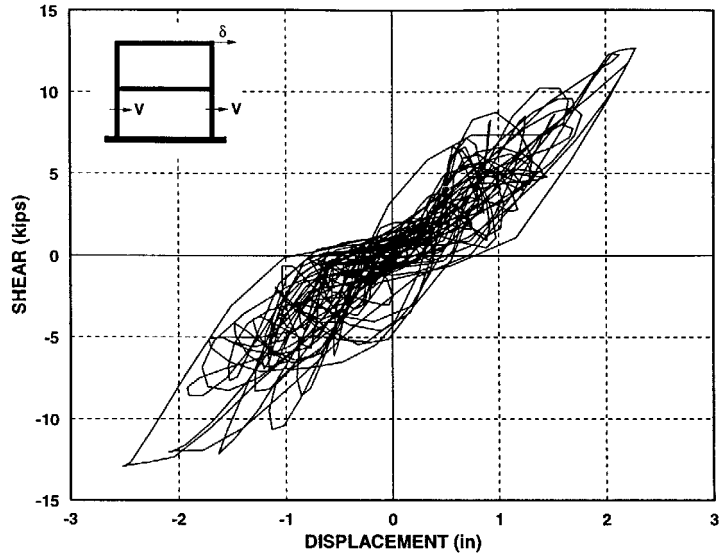


Figure 8(a). Bottom-storey shear-top-storey displacement relation with bar slip effect

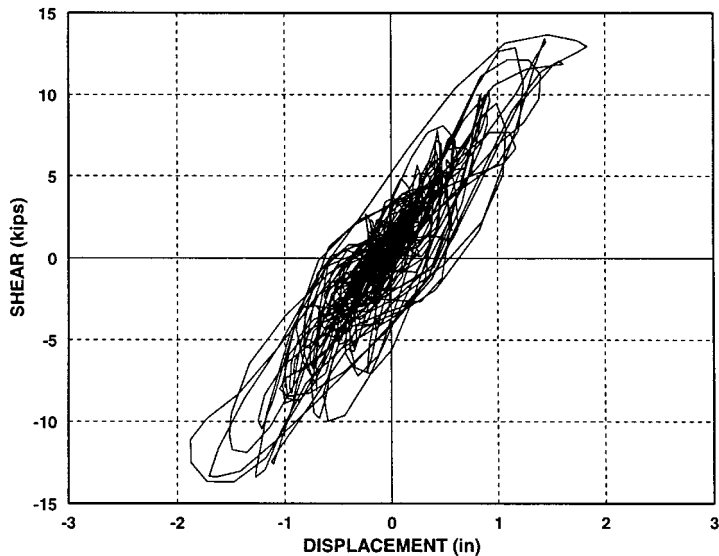


Figure 8(b). Bottom-storey shear-top-storey displacement relation without bar slip effect

dissipation, damage and stiffness deterioration of the frame members. Figures 7(c) and 7(d) show that the top- and bottom-storey shear is not much affected by the effect of reinforcing bar slip. There is only a slight increase in storey shear when the effect of reinforcing bar slip is included in the analysis. This is not surprising when the storey shear force is regarded as the product of stiffness and interstorey displacement. The inclusion of joint rotations increases the fundamental period of the frame and results in larger storey displacements, while, at the same time, it decreases the lateral storey stiffness. These two effects appear to cancel out in the case of test frame RCF2, as is evident in Figures 7(c) and 7(d).

Figures 8–10 provide further details on the response of test frame RCF2. Figure 8 shows the hysteretic relation between top-storey displacement and bottom-storey shear. The out-of-phase character of these two variables results in a very irregular relation, which nonetheless shows clearly the difference in energy dissipation between the model that includes the effect of fixed-end rotations and the model that does not. Figure 9 shows the hysteretic relation between bottom-storey displacement and bottom-storey shear and is a direct reflection of the hysteretic behaviour of the bottom-storey where most damage takes place in test frame RCF2. The characteristic ‘pinching’ of the hysteretic relation as a result of reinforcing bar slip at the base of test frame RCF2 is evident in Figure 9(a). Finally, Figure 10 confirms that the top storey suffered little damage.

## CONCLUSIONS

The correlation studies of the proposed model with experimental results from the shaking-table study of the dynamic response of a two-storey, one bay RC frame prove that the model is capable of describing with satisfactory accuracy the dynamic response of reinforced concrete frame structures under severe base excitations and still retain computational efficiency.

The analytical studies demonstrate that the inclusion of fixed-end rotations at the interface of girders and columns as well as at the interface of columns and footings is essential in the dynamic response analysis of RC frame structures during the final design evaluation phase. The exclusion of the reinforcing bar slip from RC frame models leads to an underestimation of the flexibility of the frame and, thus, to an underestimation of

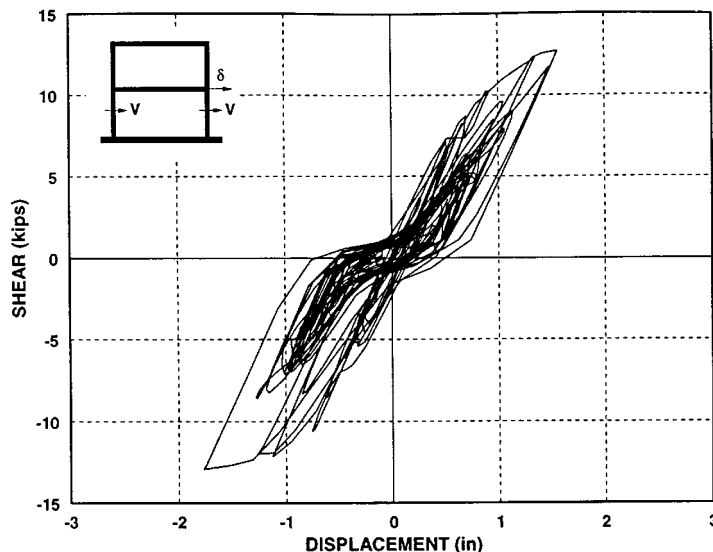


Figure 9(a). Bottom-storey shear-bottom-storey displacement relation with bar slip effect

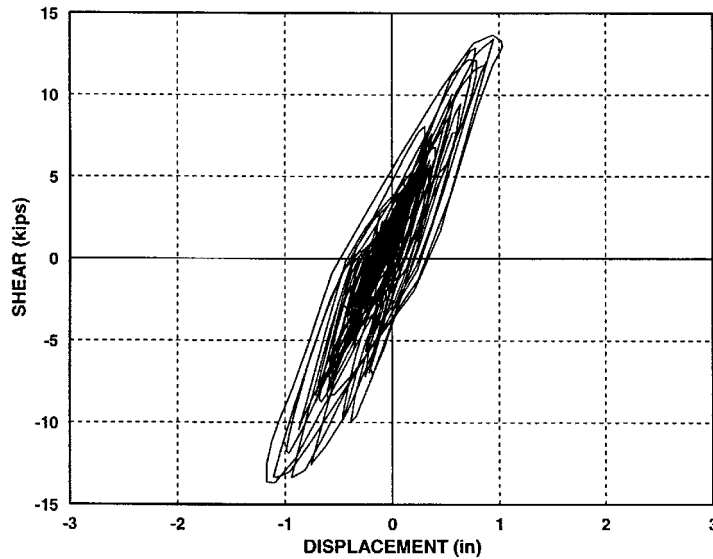


Figure 9(b). Bottom-storey shear-bottom-storey displacement relation without bar slip effect

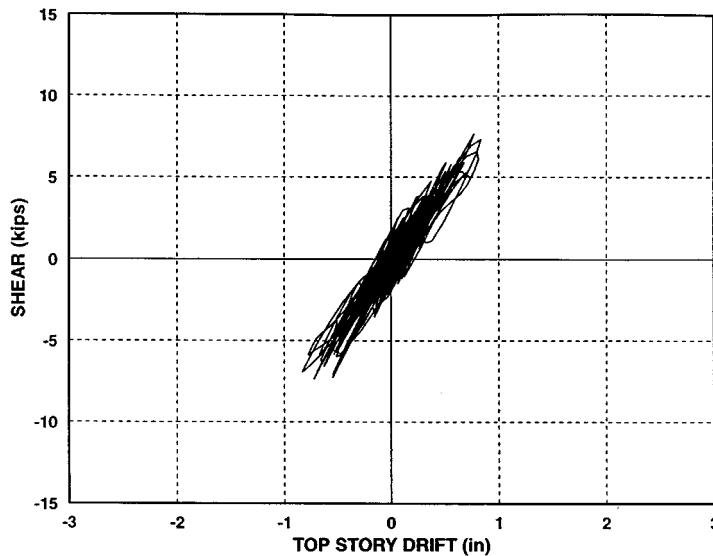


Figure 10(a). Top-storey shear-top-storey drift relation with bar slip effect

the fundamental period of the structure. The impact of this underestimation on the global dynamic response of reinforced concrete frame structures under earthquake excitations naturally depends on the relation between frequency content of excitation and dynamic properties of the structure.

The effect of reinforcing bar slip on the local response of RC frames under earthquake excitations is very significant. The energy dissipation at the joints makes up a large portion of the total energy dissipated in the

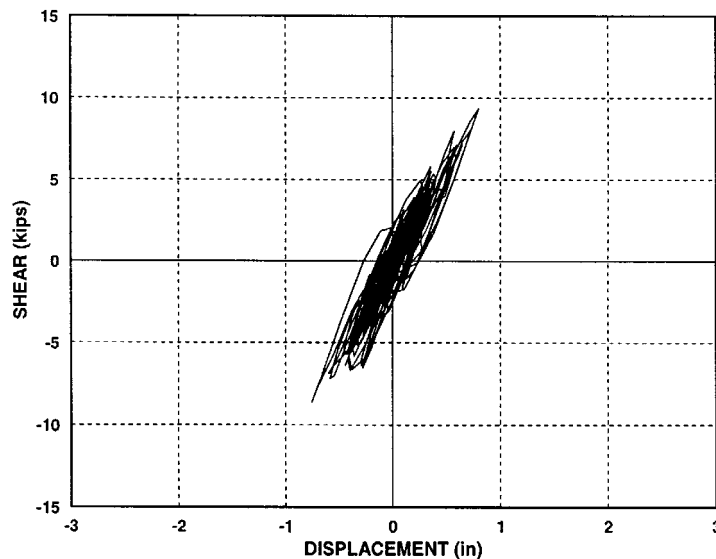


Figure 10(b). Top-storey shear-top-storey drift relation without bar slip effect

structure. Thus, beam–column and column–footing joints should be designed to have large energy dissipation capacity so as to satisfy the imposed rotation ductility demand. Furthermore, the exclusion of the effect of reinforcing bar slip in the non-linear dynamic analysis of RC frames leads to an overestimation of the flexural rotation of frame members.

#### ACKNOWLEDGEMENTS

This report is part of a larger study on the seismic response of reinforced concrete structures supported by Grant ECE-8657525 from the National Science Foundation. This support is gratefully acknowledged. Any opinions expressed in this report are those of the authors and do not reflect the views of the sponsoring agency. The first author expresses his appreciation to Professor A. Di Tommaso for his support of the stay at UC Berkeley. The financial support of this stay by the Italian Consiglio Nazionale di Ricerca (CNR) under Contract No. 94-01898-CT07 is gratefully acknowledged.

#### REFERENCES

1. C. Meyer and H. Okamura, 'Finite element analysis of reinforced concrete structures', *US–Japan Joint Seminar on Finite Element Analysis of Reinforced Concrete*, Tokyo, Japan, 1985.
2. J. C. Anderson and W. H. Townsend, 'Models for RC frames with degrading stiffness', *J. struct. engng. ASCE* **103** (1977).
3. T. Takayanagi and W. C. Schnobrich, 'Non linear analysis of coupled wall systems', *Earthquake Engng. Struct. Dyn.* **7**, 1–22 (1979).
4. H. Umemura and H. Takizawa, *Dynamic Response of Reinforced Concrete Buildings*, International Association of Bridge and Structural Engineering, Zürich, Switzerland, 1982.
5. V. V. Bertero, 'Seismic behavior of structural concrete linear elements (beams, columns) and their connections', *Introductory Report to Theme II, AICAP-CEB Symp., Structural concrete under seismic actions*, Rome, 1979, pp. 125–212.
6. F. C. Filippou, A. d'Ambrisi and A. Issa, 'Nonlinear static and dynamic analysis of RC subassemblages', *UCB/EERC-92/08*, Earthquake Engineering Research Center, University of California, Berkeley, 1992.
7. R. W. Clough and J. Gidwani, 'Reinforced concrete frame 2: testing and analytical correlation', *UCB/EERC-76/15*, Earthquake Engineering Research Center, University of California, Berkeley, 1976.
8. R. W. Clough, and J. Penzien, *Dynamics of Structures*, McGraw-Hill, New York, 1975.
9. M. F. Giberson, 'Two nonlinear beams with definition of ductility', *J. struct. div. ASCE* **95** (ST7) (1974).
10. F. C. Filippou and A. d'Ambrisi, 'Effect of local detailing on the seismic response of reinforced concrete structures', *10th European conf. on earthquake engineering*, Vienna, 1994.

11. J. M. Blondet, R. W. Clough and S. A. Mahin, 'Evaluation of a shaking table test program on response behavior of a two story reinforced concrete frame', *EERC 80-42*, Earthquake Engineering Research Center, University of California, Berkeley, 1980.
12. C. Meyer, M. S. L. Roufaiel and S. G. Arzoumanidis, 'Analysis of damaged concrete frames for cyclic loads', *Earthquake Engng. Struct. Dyn.* **11**, 207–228 (1983).
13. E. Spacone, F. C. Filippou and F. F. Taucer, 'Fiber beam–column model for nonlinear analysis of RC Frames: II: Applications', *Earthquake Engng. Struct. Dyn.* **25**, 727–742 (1996).
14. R. Park and T. Paulay, *Reinforced Concrete Structures*, Wiley, New York, 1975.
15. F. C. Filippou, 'A simple model for reinforcing bar anchorages under cyclic excitations', *J. struct. engng. ASCE* **112** (ST7), 1639–1659 (1986).
16. F. C. Filippou, E. P. Popov and V. V. Bertero, 'Modeling of reinforced concrete joints under cyclic excitations', *J. struct. engng. ASCE* **109**, 2666–2684 (1983).
17. F. C. Filippou and A. Issa, 'Nonlinear analysis of reinforced concrete frames under cyclic load reversals', *UCB/EERC-88/12*, Earthquake Engineering Research Center, University of California, Berkeley, 1988.